

SUCCESSIVE CONVEXIFICATION-BASED FUEL-OPTIMAL HIGH-ALTITUDE GUIDANCE OF THE RETALT REUSABLE LAUNCHER

Fabio Spada⁽¹⁾, Pietro Ghignoni⁽²⁾, Afonso Botelho⁽³⁾, Gabriele De Zaiacomo⁽⁴⁾, Paulo Rosa⁽⁵⁾

⁽¹⁾*Deimos Engineering and Systems S.L.U., fabio.spada@deimos-space.com*

⁽²⁾*Deimos Engineering and Systems S.L.U., pietro.ghignoni@deimos-space.com*

⁽³⁾*Deimos Engenharia, afonso.botelho@deimos-space.com*

⁽⁴⁾*Deimos Engineering and Systems S.L.U., gabriele.dezaiacomo@deimos-space.com*

⁽⁵⁾*Deimos Engenharia, paulo.rosa@deimos-space.com*

ABSTRACT

The present work discusses a solution for the High-Altitude Guidance (HAG) problem for reusable rockets. Two of the main concerns associated with it are assessed in this work: managing uncertainties while minimizing the expense of fuel and computing onboard a trajectory that the controller can track. Successive convexifications (SCvx) are widely employed for both purposes. The first problem is addressed offline; uncertainties on the initial mission conditions are optimally handled through the offline generation of a lookup table scheduling ignition height and attitude for the start of the powered phase. A SCvx-based algorithm generates guesses for an indirect shooting, which ultimately solves the FO reentry problem; the scheme employed to generate the lookup table is hence dubbed *Hybrid*. The second problem is addressed by solving online, at the height evaluated with the LUT, a nonlinear formulation of the FO reentry problem with an algorithm entirely based on SCvx. Such scheme integrates with a zero-order hold scheme the translational dynamics, the pitch and yaw kinematics and the thrust magnitude dynamics, hence it is referred to as *Augmented Quasi-5DoF*. The two techniques are combined on the benchmark of the high-lift launch vehicle RETALT1 (RETro propulsion Assisted Landing Technologies - Two-Stage-To-Orbit vehicle) and tested in a high-fidelity simulator including a real controller and accurate gravity and atmospheric models.

1 INTRODUCTION

The last decade witnessed the major boost in space services since the beginning of space commercial activities. Development of reusable launchers has played a fundamental role in such advancement: cuts in refurbishment costs have indeed positively impacted on the financial needs to access stable operational orbits. In this context, the EU and ESA have made increasing efforts to achieve the goal of making launcher reusability the state of the art in Europe. One such effort is RETALT (RETro Propulsion-Assisted Landing Technologies), a Horizon 2020 project that allowed to increase the TRL of key technologies that will enable retro propulsion-assisted launcher reusability in Europe [1]. In particular, one of the enabling technologies for launchers' recovery through vertical landing is indeed autonomous GNC: a GNC solution was developed and brought to TRL3 in RETALT, concerning both the Navigation and the Guidance & Control (G&C) area. With respect to the latter, it was opted for guiding the rocket using exact deterministic models, and for controlling it with disturbance-tolerant control laws [2]. As a consequence, convex optimization leveraging reduced-accuracy models [3] was chosen to deal with pinpoint landing conditions while ensuring optimization convergence [4]; H_∞ was

instead used to synthesize structured controllers capable of rejecting environmental uncertainties and tracking the reference prescribed by the optimization-based guidance [2]. Such approaches, which offer robustness per se, may however get weaker when interacting in the complete G&C block. The present work, therefore, constitutes a step towards a more harmonised G&C; the proposed solutions are applied to the re-entry burn problem for RETALT1: it constitutes a valid case study, as dispersions in conditions at Main-Engine Cut Off (MECO), *i.e.* stage separation, are not corrected prior to the re-entry burn; as burn occurs approximately 250 s after stage separation, dispersions heavily stress the G&C robustness.

For what concerns harmonisation of Guidance and Control logics, a first issue arises if the reference prescribed by the guidance requires action beyond the real control actuation limits. This problem may arise due to mismatch either between the plant modelled in the guidance and the real one, or between the nominal and the off nominal operating conditions of the vehicle. Different approaches have been suggested in literature to overcome this problem. A first, the most radical one, fuses the Guidance and Control functions in a single G&C block: in this fashion, Learning techniques offer time-cheap mapping from state to action [5], [6]; a different formulation of the optimization problem, dubbed Desensitized Optimal Control, allows instead to estimate the control gains every time the guidance provides a reference trajectory [7], [8]. Deterministic convex guidance schemes, making up a second approach, insist instead on the mantra 'Model a plant as accurately as possible, as long as its dynamics can be convexified'; they retain the Control as separated from the Guidance, and have been applied to landing problems in different environments [9]–[13]. A last third approach treats the Stochastic Optimal Control problem [14], with successive convexifications as candidate scheme for solving it onboard [15]. In this work the second research line is followed: the Fuel-Optimal (FO) powered re-entry problem of RETALT is transcribed with an *Augmented Quasi-5DoF* (AQ5DoF) scheme, *i.e.* a scheme integrating translational dynamics, pitch and yaw angles kinematics and thrust magnitude dynamics. This open final time problem is treated with Successive convexifications [16]: computational time requirements are hence met without sacrificing convergence insurance. With respect to similar suggested solutions [9], the roll angle is ignored, as the thrust force is the dominant contribution and is singular with respect to roll command in first approximation. In addition, we propose a zero-order hold (ZOH) for integrating the system as it constitutes a valid trade-off between accuracy and computational time [17].

A second important bottleneck appears if changes in guidance modes are scheduled with fixed position, *e.g.* triggering a landing burn when a certain fixed height is reached; the guidance may not be able to generate a feasible trajectory at all. Indeed, when deviations from nominal Initial Conditions (ICs) are too high, control authority modelled in the guidance scheme may not suffice to 'close' the trajectory at the prescribed target. It is possible to impose the final conditions as soft constraints, thus formulating the Optimal Control Problem as the problem of minimizing deviations from target [18]; such solution, however, does not provide an a-priori evaluation of the final deviation. A few algorithms, instead, schedule online the guidance mode change, thus granting feasibility while further improving fuel consumption [10], [19]. An adaptive ignition-height scheme is suggested in this work. Rather than optimizing ignition height online, a Lookup Table (LUT) based on the most critical uncertainties at MECO ICs is compiled offline. Such LUT allows to schedule both ignition height and attitude: ignition height is fundamental not only to grant feasibility, but to minimize as well fuel consumption; at ignition, instead, a correct initial orientation of the rocket is of utmost importance to allow the controller to track the prescribed trajectory. A Hybrid convex-indirect scheme is employed to compile the LUT [20]: it is based on an indirect shooting [21] warm-started with a pseudospectral convex algorithm [22]. An analytical Covector Mapping Theorem grants the accuracy of the warm starting [23].

The present paper is organized as follows. Sec. 2 provides an overview of the employed offline and

online guidance schemes; justifications on the main choices concerning both of them are provided as well. In Sec. 3 the offline ignition scheduling approach is deepened: Sec. 3.1 describes the employed optimal control formulation, Sec. 3.2 provides an overview of the convex-indirect hybrid algorithm used to solve it whereas Sec. 3.3 outlines the ignition scheduling strategy. Contents in Sec. 4 follow a similar structure as for the previous section: Sec. 4.1 describes the non-convex AQ5DoF powered descent problem while the online successive convexification-based algorithm is described in Sec. 4.2. The guidance algorithms are tested within a high-fidelity simulator, with a controller in the loop. Relative results are outlined in Sec. 5: firstly, a Monte-Carlo analysis validates the proposed offline scheduling method; in second instance the proposed quasi 5-DoF scheme is tested for nominal MECO conditions. Conclusions and future development directions are presented in Sec. 6.

2 TRAJECTORY PLANNING OVERVIEW

The present work is focused on the *High-Altitude Guidance* (HAG) of a reusable rocket. HAG involves the *reentry burn*: it allows to target the initial state of the *aerodynamic descent* exactly (ignoring for simplicity the navigation errors), whilst tackling existing dispersions at Main-Engine Cut Off (MECO). The G&C strategy is depicted in Fig. 1; the guidance problem is formulated in the East-North-Up (ENU) topocentric reference frame, centered on the landing barge, and referred to as x - y - z in Fig. 1. First phase, i.e. the *flip over*, is used to bring thrusters upwind, preparing for the reentry burn; the second phase is a pure *ballistic flight* during which attitude is controlled and kept constant, while the third effectively consists of the reentry burn. With reference to Fig. 1, let us focus at first

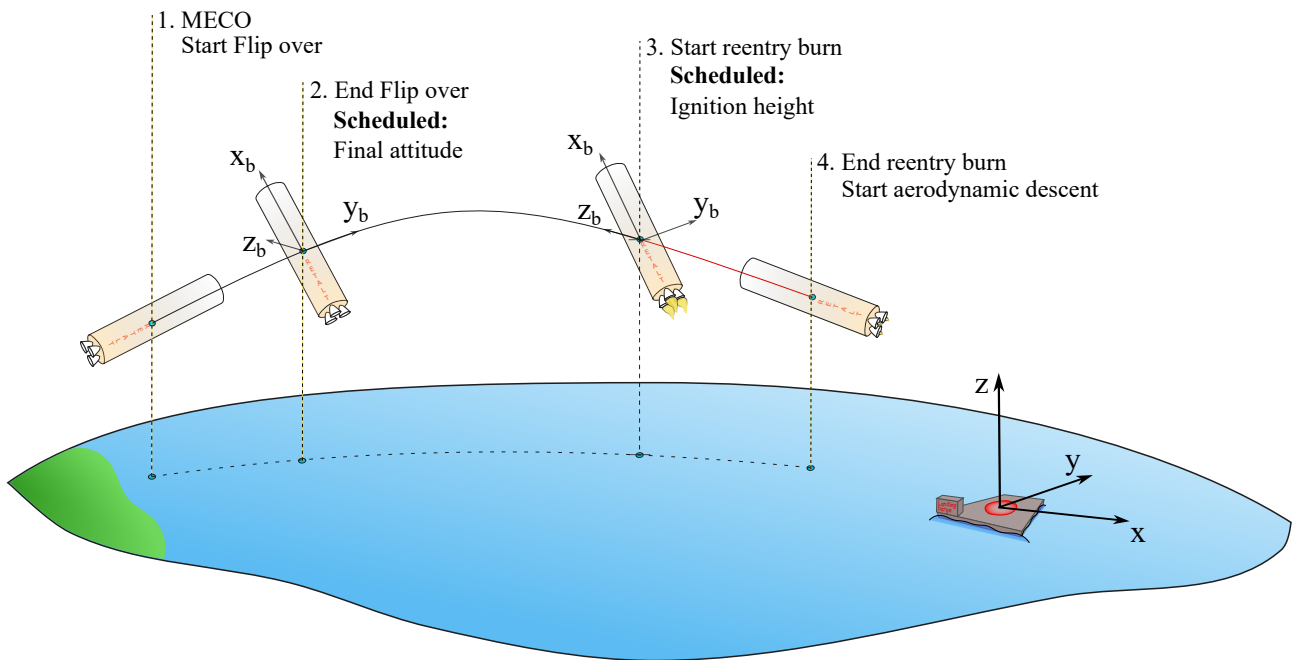


Figure 1: Overview of the High-Altitude Guidance strategy - *Not to scale*

on the red trajectory arc, the powered reentry phase. Dispersions at MECO conditions determine the real trajectory to severely deviate from the nominal one. As a consequence, controllability may be achieved as long as guidance is performed in closed-loop fashion; convex optimization algorithms provide a valid and applied tool to solve this problem [24], [25] while allowing, up to a certain degree, to minimize expended fuel. A first design choice, therefore, consists of employing convex algorithms to generate a reference trajectory for the reentry burn. A nearly 5-DoF guidance algorithm based on successive convexifications of the original non-convex problem is employed for this purpose: nearly

5-DoF guidance allows to directly include attitude rates limitations in the trajectory planning, while successive convexifications offer a versatile approach for treating non-convex constraints with convex solvers.

Still referring to Fig. 1, the focus shall be now moved to quantities referred to as **Scheduled**: given a discrete number of MECO conditions, the scheduled quantities are optimized offline; a Lookup Table (LUT) built on such computed values is then used by the on-board software. Need for such scheduling is now outlined. Let us consider nominal MECO conditions; in this case, a certain ignition height $h_{\text{ign},0}$ optimizes fuel consumption during the reentry burn. However, for different dispersed MECO conditions, as ground speed magnitude v^M or heading χ^M , a feasible powered trajectory triggered at $h_{\text{ign},0}$ may not exist at all. Picture in Fig. 2 depicts how this problem affects the case study of RE-TALT, for fixed ignition height $\bar{h}_{\text{ign},0} = 75$ km. Trajectory in black is the nominal one; the others are

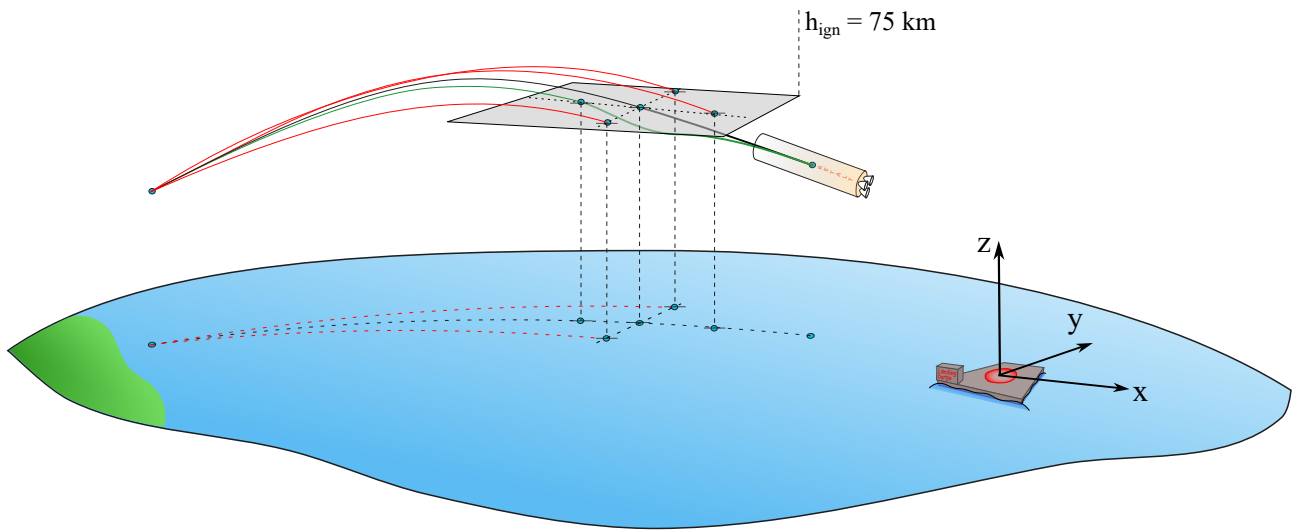


Figure 2: Nominal trajectory, feasible and unfeasible dispersed trajectories - *Respectively in black, green and red* - for dispersed MECO ground speed and heading and for fixed ignition height reentry burn - *Not to scale*

associated with dispersions in v^M or χ^M : dispersed v^M determines errors in the downrange direction, dispersed χ^M induce crossrange errors. Trajectory colors indicate whether a reentry burn arc (in bold in Fig. 2) triggered at $\bar{h}_{\text{ign},0}$ allows or not to target the initial conditions of the aerodynamic descent; respectively green indicate feasible trajectories, red an unfeasible one. The considered deviations are with 3σ uncertainty. Adapting ignition height to MECO conditions is therefore evident: we opt for scheduling ignition height for $\pm 3\sigma$ in v^M only, in χ^M only and in the combined cases. Scheduled heights grant feasibility while minimizing fuel consumption during reentry burn. In addition, the optimal attitude required by the guidance scheme at the beginning of the reentry burn $e\mathbf{a}_0^*$ changes sensitively depending on MECO conditions. In the same fashion as for ignition height, $e\mathbf{a}_0^*$ is therefore evaluated for fixed number of MECO conditions; flip-over maneuver, therefore, targets $e\mathbf{a}_0^*$ as final attitude, which is maintained constant during the *ballistic arc*, i.e. up to the scheduled $h_{\text{ign},0}$.

3 IGNITION OFFLINE SCHEDULING

3.1 3-DoF Fuel-Optimal descent problem formulation

Hereinafter the following notation is employed, if not differently specified: boldface italic letters and their lightface counterpart respectively denote vectors in \mathbb{R}^3 and their Euclidean norm; vectors are intended as column vector, independently on their dimensions. Lightface italic letters indicate as well scalar parameters.

The offline scheduling algorithm solves the 3-DoF free final time FO powered pinpoint re-entry problem. Let the state $\mathbf{x} \in \mathbb{R}^7$ gather the position \mathbf{r} , speed \mathbf{v} expressed in the landing-site centered East-North-Up (ENU) reference frame and mass m according to $\mathbf{x} \doteq [\mathbf{r}^T, \mathbf{v}^T, m]^T$. In addition, let u_T and \mathbf{i}_T respectively denote the normalized thrust and its direction. The Fuel-Optimal pinpoint reentry problem reads as in Eq. (1)

$$\min_{u_T, \mathbf{i}_T, t_f} \mathcal{J} \quad \text{s.t.} \quad \begin{cases} \dot{\mathbf{x}} = \mathbf{f}(\mathbf{x}, u_T, \mathbf{i}_T) \\ \mathbf{x}_0 = \bar{\mathbf{x}}_0 \\ \mathbf{r}_f = \bar{\mathbf{r}}_f \\ \mathbf{v}_f = \bar{\mathbf{v}}_f \\ u_{T, \min} \leq u_T \leq u_{T, \max} \\ \mathbf{i}_T = 1 \end{cases} \quad (1)$$

where $\mathbf{f} \in \mathbb{R}^7$ represents the flat-Earth constant gravity 3-DoF powered-rocket dynamics and \mathcal{J} defines the thrust-acceleration integral along the burning arc. The pure control path constraint $u_{T, \min} \leq u_T \leq u_{T, \max}$ is associated with engine throttling limits, while $\mathbf{i}_T = 1$ stems from definition of \mathbf{i}_T as unit vector.

Strictly speaking, problem in Eq. (1) does correspond to the Acceleration-Optimal formulation of the pinpoint reentry problem. Nonetheless, use of variational mathematics allows to demonstrate the optimal control profile solving Eq. (1) coincides with the Fuel-Optimal thrust profile [26].

3.2 Hybrid convex-indirect algorithm

Problem in Eq. (1) can be solved quickly and accurately, provided that 1) an accurate optimization algorithm is used and 2) such algorithm is started with an accurate guess. With respect to these, a hybrid approach is employed [20]: use of a state-of-the-art indirect single shooting solves issue 1), and warm starting it with a convexified version of Eq. (1) solves issue 2). Loosely speaking, a convex pseudospectral (PS) collocation provides an estimation of the costates solving the indirect shooting. Effectiveness of the warm starting is guaranteed by an analytical Covector Mapping Theorem [27] that characterizes the Radau-Pseudospectral method [23] underlying the pseudospectral convex collocation [22]. In addition, the convex collocation employs a free final time formulation to further grant robustness to the warm starting. The pipeline of the complete hybrid algorithm is reported in Fig. 3. For length limitations, however, the present subsection has been compressed; the interested reader is suggested to consult the original contribution in which such algorithm has been proposed [20].

3.2.1 Pseudospectral free final time convex collocation

Transcribing problem in Eq. (1) to the mentioned free-final-time convex formulation requires three steps; the solved Pseudospectral free final time convex collocation problem is outlined in the third bullet point.

1. *Convex relaxation* [26]: Such step introduces linear dynamics $\mathbf{f}_{\text{cvx}} \in \mathbb{R}^7$ and a linear objective function \mathcal{J}_{cvx} via the change of variables in Eq. (2).

$$\mathbf{u} \doteq u_T \frac{T_{\max}}{m} \mathbf{i}_T, \quad \sigma \doteq u_T \frac{T_{\max}}{m}, \quad \tilde{m} \doteq \log(m) \quad (2)$$

The obtained dynamics Right-Hand Side $\mathbf{f}_{\text{cvx}}(\mathbf{x}_{\text{cvx}}, \mathbf{u}, \sigma)$, where $\mathbf{x}_{\text{cvx}} \doteq [\mathbf{r}^T, \mathbf{v}^T, \tilde{m}]^T$, is linear in the states and controls, as well as \mathcal{J}_{cvx} .

The non-convex equality constraint $\mathbf{i}_T = 1$ in Eq. (1) is then *relaxed* to its convex counterpart,

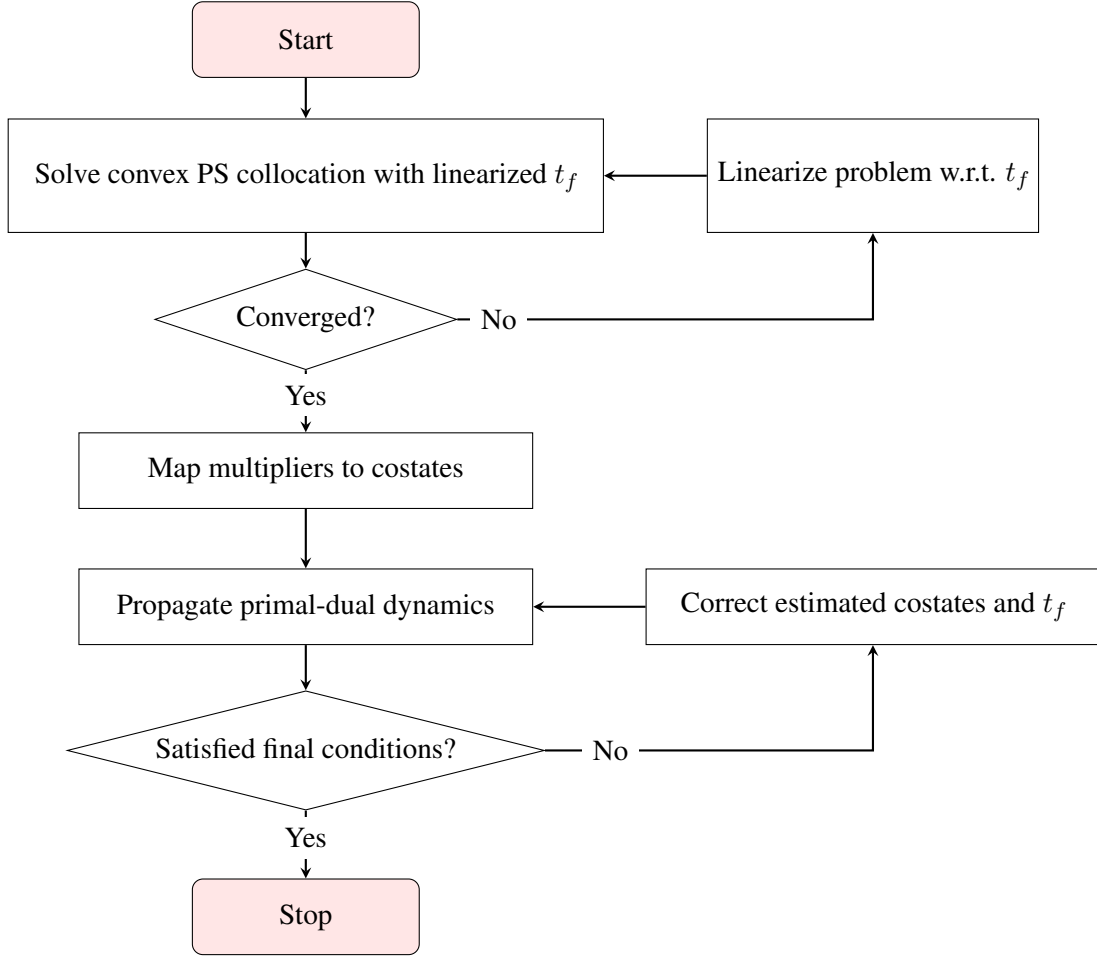


Figure 3: Hybrid convex-indirect algorithm employed to generate the Lookup Table for ignition height

obtaining constraints that can be treated with off-the-shelf Second Order Conic (SOC) solvers [28].

Eq. (1) is therefore turned into Eq. (3).

$$\min_{\mathbf{u}, \sigma, t_f} \mathcal{J}_{\text{cvx}} \quad \text{s.t.} \quad \begin{cases} \dot{\mathbf{x}}_{\text{cvx}} = \mathbf{f}_{\text{cvx}}(\mathbf{x}_{\text{cvx}}, \mathbf{u}, \sigma) \\ \text{Relaxed } i_T = 1 \\ \mathbf{x}_{\text{cvx},0} = \bar{\mathbf{x}}_{\text{cvx},0} \\ \mathbf{r}_f = \bar{\mathbf{r}}_f \\ \mathbf{v}_f = \bar{\mathbf{v}}_f \end{cases} \quad (3)$$

2. *Pseudospectral hp transcription*: Problem in Eq. (3) is then transcribed according to a Legendre-Gauss-Radau (LGR) scheme. This allows to transform the non-convex expression $\dot{\mathbf{x}}_{\text{cvx}}$ to its convex pseudospectral approximation, by introducing the *pseudospectral differential operator* $\mathbf{D} \in \mathbb{R}^{n \times (n+1)}$, given that $n + 1$ defines the number of discretization points the subdomains, called *segments*, are subdivided in. For equal segments and fixed time \bar{t}_f , \mathcal{J}_{cvx} is instead transcribed according to Eq. (4), where p defines the number of *segments* and w_i the *pseudospectral integration weights*.

$$\mathcal{J}_{\text{cvx}}^{hp} \doteq \frac{\bar{t}_f}{2p} \sum_{j=1}^p \sum_{i=0}^n w_i \sigma_i^j \quad (4)$$

Problem obtained in such manner can be solved in one iteration, for fixed final time. The interested reader is referred to [22] for further mathematical details.

3. *Successive convexifications of non-convex free final time contributions*: Last step consists in restoring \bar{t}_f as optimization variable. This is done by iteratively linearizing with respect to t_f the constraints and $\mathcal{J}_{\text{cvx}}^{\text{hp}}$ in Eq. (4) and solving the corresponding problem. The procedure is repeated up to convergence of the final time.

More specifically, as $\mathbf{X}_{\text{cvx},i}^j$ and \mathbf{U}_i^j define states and controls at i^{th} node of j^{th} segment, at the $(k+1)^{\text{th}}$ iteration the dynamics constraints read as in Eq. (5) and the objective function as in Eq. (6). The terms with superscript $(\cdot)^{(k)}$ are the solution of the previous iteration, therefore Eq. (5) and Eq. (6) are linear with respect to both states, controls and t_f .

$$\frac{2p}{t_f^{(k)}} \mathbf{D}_i \mathbf{X}_{\text{cvx}}^j = \mathbf{f}_{\text{cvx}}(\mathbf{X}_{\text{cvx},i}^j, \mathbf{U}_i^j) + \frac{2}{(t_f^{(k)})^2} \mathbf{D}_i \mathbf{X}_{\text{cvx}}^{(k)} (t_f - t_f^{(k)}) \quad \text{with} \quad \begin{array}{l} i = 0, \dots, n-1 \\ j = 1, \dots, p \end{array} \quad (5)$$

$$\mathcal{J}_{\text{cvx}}^{\text{hp}} = \frac{t_f^{(k)}}{2p} \sum_{j=1}^p \sum_{i=0}^n w_i \sigma_i^j + \frac{1}{2p} \sum_{j=1}^p \sum_{i=0}^n w_i \sigma_i^{(k),j} (t_f - t_f^{(k)}) \quad (6)$$

3.2.2 Costates extraction

Once the convex pseudospectral problem is solved, the Lagrange multipliers of dynamics constraints at the initial time $\Lambda_0^1 \in \mathbb{R}^7$ are isolated and mapped to the corresponding costates $\tilde{\lambda}_0 \in \mathbb{R}^7$ according to Eq. (7) [23], where $\tilde{\lambda}_0$ gathers the initial *coposition* $\lambda_{r,0}$, *cospeed* $\lambda_{v,0}$ and *logarithmic comass* $\lambda_{\tilde{m},0}$ according to $\tilde{\lambda}_0 \doteq [\lambda_{r,0}^T, \lambda_{v,0}^T, \lambda_{\tilde{m},0}]^T$. $\lambda_{\tilde{m},0}$ is then mapped to $\lambda_{m,0}$ using the derivation proposed in [29].

$$\tilde{\lambda}_0 = \frac{\Lambda_0^1}{w_1} \quad (7)$$

3.2.3 Indirect single shooting

It is possible to solve Eq. (1) finding the control profile and t_f satisfying its first-order optimality necessary conditions [30]. The associated problem is outlined in Eq. (8) and solved by the indirect single shooting. Indeed, by employing *Pontryagin's Minimum Principle* (PMP) [31], the initial OCP is firstly transformed into a *Two-Point Boundary Value Problem* (TPBVP) [32]; this TPBVP is then recast as the *Initial Value Problem* outlined in Eq. (8).

$$\text{Find } [\lambda_0^T, t_f]^T \text{ s.t. } \mathbf{y}(t) \text{ satisfies } \Xi = \mathbf{0}, \text{ given } \Xi(\lambda_0, t_f) \doteq \begin{bmatrix} \mathbf{r}(\lambda_0, t_f) - \bar{\mathbf{r}}_f \\ \mathbf{v}(\lambda_0, t_f) - \bar{\mathbf{v}}_f \\ \lambda_m(\lambda_0, t_f) \\ \mathcal{H}(\lambda_0, t_f) \end{bmatrix} \in \mathbb{R}^8 \quad (8)$$

where the *Hamiltonian* \mathcal{H} is evaluated for the optimal control profile u_T^* computed through the PMP [31]. $\mathbf{y} \in \mathbb{R}^{14}$ gathers instead the primal-dual states according to $\mathbf{y} \doteq [\mathbf{x}^T, \boldsymbol{\lambda}^T]^T$. The essence of the indirect shooting lies in solving iteratively problem in Eq. (8) by first *propagating* the guessed λ_0 and t_f with the dynamics in defined by optimal controls u_T^* and \mathbf{i}_T^* [33], then by *correcting* these guesses nulling the resulting constraints violation (i.e. constraints in Eq. (8)).

1. *Correction step*: For correction purposes, constraints are approximated with a first-order differential expression based on their analytical Jacobian $\mathbf{J}_{[\lambda_0, t_f]} \Xi \in \mathbb{R}^{8 \times 8}$; the solution λ_0 and t_f

at each step k_m is found by solving Eq. (9), where $\lambda_0^{k_m}$ and $t_f^{k_m}$ are the guesses at the corresponding iteration. Notice $\Xi(\lambda_0^{k_m}, t_f^{k_m})$ is computed propagating the guessed costates $\lambda_0^{k_m}$ up to guessed final time $t_f^{k_m}$.

$$\Xi(\lambda_0, t_f) \approx \Xi(\lambda_0^{k_m}, t_f^{k_m}) + \mathbf{J}_{[\lambda_0, t_f]}^{k_m} \Xi \begin{bmatrix} \lambda_0 - \lambda_0^{k_m} \\ t_f - t_f^{k_m} \end{bmatrix} = \mathbf{0} \quad (9)$$

Constraints' Jacobian $\mathbf{J}_{[\lambda_0, t_f]}^{k_m} \Xi$ is defined using the *State Transition Matrix* (STM) $\Phi \in \mathbb{R}^{14 \times 14}$. $\mathbf{J}_{[\lambda_0, t_f]}^{k_m} \Xi$ has been defined analytically in [20], while details on the STM can be found in [33].

2. *Propagation step*: As consequence of how constraints have been approximated, the propagation step deals with an augmented dynamics involving both the primal-dual states and the STM. Since discontinuities in the control profile [34] imply discontinuities in the primal-dual dynamics, jumps in the STM components are evaluated at every *bang* of the control according to [33].

3.3 Lookup table generation

Machinery described in Sec. 3.2 solves a fixed-initial height problem; however, as an optimal height is pursued, the FO descent problem is solved for different h_0 values. The algorithm in Fig. 3 is run once for a high value of h_0 to grant finding a feasible solution. A sequence of indirect shootings obtained for decreasing h_0 values is then triggered; with reference to Fig. 4, each line represents one such sequence. Each subproblem of the sequence obtained for varying h_0 has its guess initialized with the solution of the previous subproblem. h_0 is decreased up to when infeasibility is detected; the optimal height h_0^* is then extracted. An example of the procedure is outlined in Fig. 4: on y-axis is reported the ignition height, on the x-axis the fuel consumption of the corresponding re-entry burn arc. Each line corresponds to a specific initial condition at cutoff. Fixing χ^M to its nominal value of 94.64° , v^M varies in Fig. 4 between the nominal of 2217 m s^{-1} and the $+2\sigma = 50 \text{ m s}^{-1}$ dispersion: feasibility lower limits vary of 20 km approximately. In case of $+2\sigma$ of v^M , igniting at the optimal height of the nominal case would therefore be infeasible.

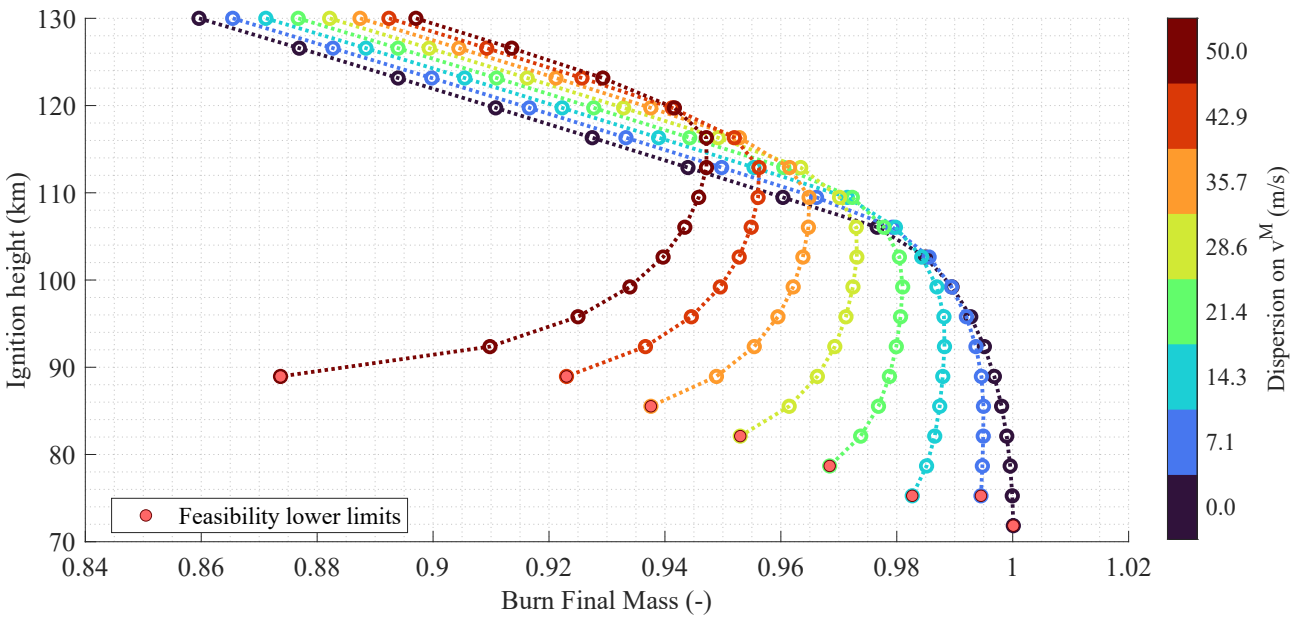


Figure 4: Mass burnt during re-entry burn as function of ignition height, fixed nominal MECO heading and nominal speed dispersed in range $[0, +2\sigma]$

Hypothesizing the rocket body as aligned with rocket thrust, attitude at ignition is further extracted. Indeed, the Flip Over targets by design the initial attitude required for the reentry burn by the online-running algorithm; as a consequence, an estimate of such attitude shall be available to the onboard computer. Scheduling attitude as function of MECO conditions is compulsory, as attitude proves sensitive to errors both in downrange and crossrange directions.

At last, it is worth adding a last building block: landing the rocket is the ultimate goal, and this is achievable as long as control is granted along all reentry flight phases. In this context, limiting the angle of attack α during the reentry guidance proves useful as it allows to implicitly limit the disturbance from aerodynamic forces. Specifically, a limitation as in Fig. 5 allows to selectively constrain flight at lower heights, where aerodynamic disturbances are more intense. Trajectory in

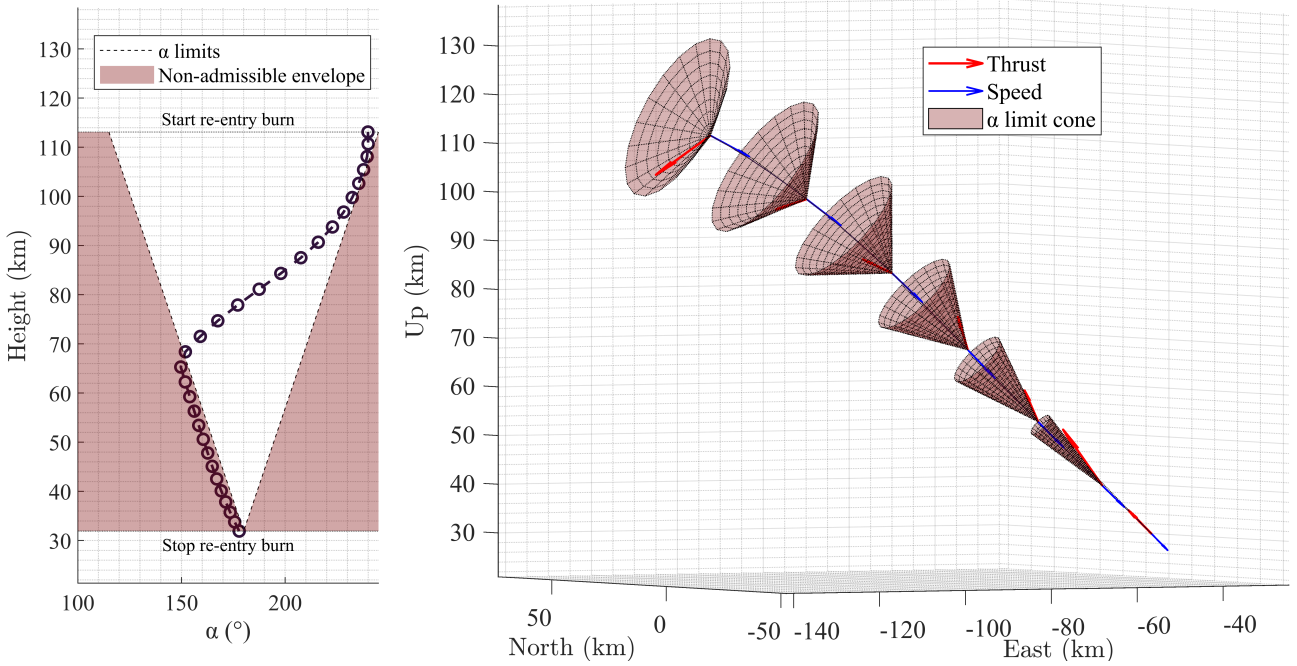


Figure 5: α limitation along re-entry arc

Fig. 5 corresponds to nominal χ^M and $+2\sigma$ in v^M . Constraining α influences the initial attitude of the reentry burn: the optimal solution for each couple of dispersed v^M, χ^M is further processed with a convex solver implementing the angle of attack constraint, and the attitude Lookup Table run onboard is compiled with such last data.

4 ONLINE GUIDANCE STRATEGY

4.1 Augmented Quasi 5-DoF Fuel-Optimal descent problem formulation

The online scheduling algorithm solves the Augmented Quasi 5-DoF free final time FO powered pin-point re-entry problem, as defined in Eq. (10). Let the state $\tilde{\mathbf{x}} \in \mathbb{R}^{10}$ gather \mathbf{r} , \mathbf{v} , m , thrust yaw and pitch angles ψ and θ , and the thrust magnitude T according to $\tilde{\mathbf{x}} \doteq [\mathbf{r}^T, \mathbf{v}^T, m, \psi, \theta, T]^T$. $\dot{\mathbf{i}}_T$ is therefore computed employing a standard 3-2-1 sequence of rotations. In addition, let the control vector $\tilde{\mathbf{u}}$ gather the commanded yaw rate r_ψ , pitch rate r_θ and thrust rate r_T according to $\tilde{\mathbf{u}} \doteq [r_\psi, r_\theta, r_T]^T$.

The AQ5DoF Fuel-Optimal pinpoint reentry problem is outlined in Eq. (10).

$$\min_{\tilde{\mathbf{u}}, T_0, T_f, t_f} \tilde{\mathcal{J}} \quad \text{s.t.} \quad \begin{cases} \dot{\tilde{\mathbf{x}}} = \tilde{\mathbf{f}}(\tilde{\mathbf{x}}, \tilde{\mathbf{u}}) \\ \mathbf{r}_0 = \bar{\mathbf{r}}_0, \mathbf{v}_0 = \bar{\mathbf{v}}_0, m_0 = \bar{m}_0, \psi_0 = \bar{\psi}_0, \theta_0 = \bar{\theta}_0 \\ \mathbf{r}_f = \bar{\mathbf{r}}_f, \mathbf{v}_f = \bar{\mathbf{v}}_f, \psi_f = \bar{\psi}_f, \theta_f = \bar{\theta}_f \\ T_{\min} \leq T \leq T_{\max} \\ |\mathbf{r}_\psi| \leq r_{\psi, \max}, |\mathbf{r}_\theta| \leq r_{\theta, \max}, |\mathbf{r}_T| \leq r_{T, \max} \\ |\dot{\mathbf{r}}_\psi| \leq \dot{r}_{\psi, \max}, |\dot{\mathbf{r}}_\theta| \leq \dot{r}_{\theta, \max} \\ \alpha(\mathbf{v}, \psi, \theta) \leq \alpha_{\max}(r_z) \end{cases} \quad (10)$$

where $\tilde{\mathbf{f}} \in \mathbb{R}^{10}$ represents the flat-Earth AQ5DoF powered-rocket dynamics, according to Eq. (11)

$$\tilde{\mathbf{f}}(\tilde{\mathbf{x}}, \tilde{\mathbf{u}}) \doteq \begin{bmatrix} \mathbf{v} \\ \mathbf{a}(m, \psi, \theta, T) \\ -\tilde{\beta} T \\ \mathbf{r}_\psi \\ \mathbf{r}_\theta \\ \mathbf{r}_T \end{bmatrix} \quad \text{where} \quad \begin{cases} \mathbf{a} \doteq \frac{T}{m} \mathbf{i}_T(\psi, \theta) + \mathbf{g} \\ \tilde{\beta} \doteq \frac{1}{I_{\text{sp}} g_0} \end{cases} \quad (11)$$

and $\tilde{\mathcal{J}}$ defines the thrust magnitude integral along the burning arc as reported in Eq. (12).

$$\tilde{\mathcal{J}} \doteq \int_0^{t_f} T dt \quad (12)$$

With reference to Eq. (10), couples $\bar{\psi}_0$ and $\bar{\theta}_0$, and $\bar{\psi}_f$ and $\bar{\theta}_f$ are respectively retrieved from the real attitude and from the condition $\alpha_f = 180^\circ$. Limits associated with $|\dot{\mathbf{r}}_\psi|$ and $|\dot{\mathbf{r}}_\theta|$ provide surrogate limitations on attitude dynamics; moreover, dependency of maximum angle of attack on height mirrors the structure outlined in Fig. 5.

4.2 Online trajectory planning algorithm

It is opted for employing successive convexifications to solve problem in Eq. (10). The dynamics are integrated through a ZOH approximation, both on states and controls; continuous-time dynamics are hence converted to their corresponding discrete-time counterpart; dynamics reads as in Eq. (13) for evenly-distributed discretization points; ultimately, an even distribution is chosen, as deemed sufficient to grasp dynamics accurately.

$$\tilde{\mathbf{x}}_{i+1} = \tilde{\mathbf{x}}_i + \mathbf{F}_i(\tilde{\mathbf{x}}, \tilde{\mathbf{u}}, t_f) \quad \text{where} \quad i = 1, \dots, n_i - 1 \quad (13)$$

and n_i indicates the number of discretization points, the subscript $(\cdot)_i$ denotes the quantity in (\cdot) evaluated at i^{th} discretization point and $\mathbf{F}_i(\tilde{\mathbf{x}}, \tilde{\mathbf{u}}, t_f)$ defines the ZOH approximation of the dynamics in Eq. (11).

The obtained discrete-time optimal control problem is highly nonlinear, whilst convexification applied to equality constraints requires successive linearizations: problems of *artificial unboundedness*, due to successive linearizations, and *artificial infeasibility*, due to mismatch between the real nonlinear and the numerical linear dynamics, are prone to arise [16]. To overcome them, it is opted for using respectively soft *trust regions* and *virtual controls*.

Trust regions limit the variation of optimization variables between the generic k^{th} iteration and the following one; in case of *soft* trust regions, this is achieved by penalizing these variations in the objective function through a slack variable s_ξ ; t_f is the only variable treated with a hard constant trust

region, i.e. the variation between successive iterations is limited to a fixed value. Constraints limiting trust regions through the slack s_ξ can be solved through SOC solvers.

Virtual controls are slack variables introduced in linearized dynamics and penalized in the objective function by means of the additional slack s_ν . Constraints limiting virtual controls through the slack s_ν can be solved through SOC solvers as well.

The objective function is therefore augmented as in Eq. (14), exploiting the fixed weights w_ν, w_ξ .

$$\tilde{\mathcal{J}}_{\text{aug}} \doteq \int_0^{t_f} T dt + w_\xi s_\xi + w_\nu s_\nu \quad (14)$$

The online algorithm solves the problem defined in Eq. (10), adding the virtual controls, trust regions, and linearizing the non-convex contributions iteratively. Domain is evenly discretized, therefore allowing to have segments' lengths depend on t_f only. As an example, the linearized dynamics reads as in Eq. (15).

$$\begin{aligned} \tilde{\mathbf{x}}_{i+1} &= \tilde{\mathbf{x}}_i + \mathbf{J}_{\tilde{\mathbf{x}}_i}^{(k)} \mathbf{F}_i \tilde{\mathbf{x}}_i + \mathbf{J}_{\tilde{\mathbf{u}}_i}^{(k)} \mathbf{F}_i \tilde{\mathbf{u}}_i + \nabla_{t_f}^{(k)} \mathbf{F}_i t_f + \boldsymbol{\nu}_i + \mathbf{c}_i \\ \mathbf{c}_i &\doteq \mathbf{F}_i^{(k)} - \mathbf{J}_{\tilde{\mathbf{x}}_i}^{(k)} \mathbf{F}_i \tilde{\mathbf{x}}_i^{(k)} - \mathbf{J}_{\tilde{\mathbf{u}}_i}^{(k)} \mathbf{F}_i \tilde{\mathbf{u}}_i^{(k)} - \nabla_{t_f}^{(k)} \mathbf{F}_i t_f^{(k)} \end{aligned} \quad i = 1, \dots, n_i - 1 \quad (15)$$

where superscript $(\cdot)^{(k)}$ indicates that Jacobians and gradients are evaluated at $\tilde{\mathbf{x}}^{(k)}, \tilde{\mathbf{u}}^{(k)}, t_f^{(k)}$. Non-convex inequality constraints, namely pitch and yaw commands rates limitation and angle of attack limitation, and the objective function are successively convexified as well, similarly to what done in Eq. (15).

5 RESULTS

The described offline and online algorithms are applied to the powered re-entry guidance problem. More specifically, the kinematic quantities are here outlined, whereas the dynamical ones are left non-dimensional; lower and upper limits on non-dimensional thrust magnitude are respectively $u_{T,\min} = 0.49$ and $u_{T,\max} = 1$. Dispersions at MECO are reported in Tab. 1. Dispersions highlighted in green are employed to compile the lookup table, therefore are managed by the Guidance function directly.

Table 1: MECO dispersions - In green the ones associated with greater deviations from nominal trajectory

Physical quantity	Nominal	Standard deviation
Geodetic altitude (km)	93.06	0.8
Ground speed ($\text{m} \cdot \text{s}^{-1}$)	2217	25
Flight path angle ($^\circ$)	31.77	0.4
Heading angle ($^\circ$)	94.64	0.2

5.1 Robustness analysis

With respect to quantities highlighted in Tab. 1, the LUTs are built using the nominal and the dispersed quantities corresponding to $\pm 3\sigma$. The Lookup Table for pitch angle is reported as example in Tab. 2. Moreover, to demonstrate the effectiveness of the proposed method, a Monte-Carlo campaign is run, simulating the full scenario including a high-fidelity dynamical environment with J2-perturbed gravity model, aerodynamics, 6-DoF plant model and controller synthesized using the H_∞ technique.

Table 2: LUT for optimal ignition pitch angle[†] onboard scheduling

		Dispersed v^M		
		-3σ	Nominal	$+3\sigma$
Dispersed χ^M	$+3\sigma$	71.1°	30.2°	-31.5°
	Nominal	84.7°	33.4°	-32.1°
	-3σ	69.9°	29.6°	-31.2°

[†] Expressed with respect to landing-site centered NED reference frame

The only logic modelled as perfect is the Navigation; however, as it grants high accuracies, it has been deemed not to sensibly alter the presented results when added. Dispersions employed in the high-fidelity simulator include, besides initial conditions at MECO, the aerodynamic coefficients, the atmospheric model and vehicle inertial properties.

The 3-DoF Guidance ultimately employed to refine the attitude lookup tables limiting the angle

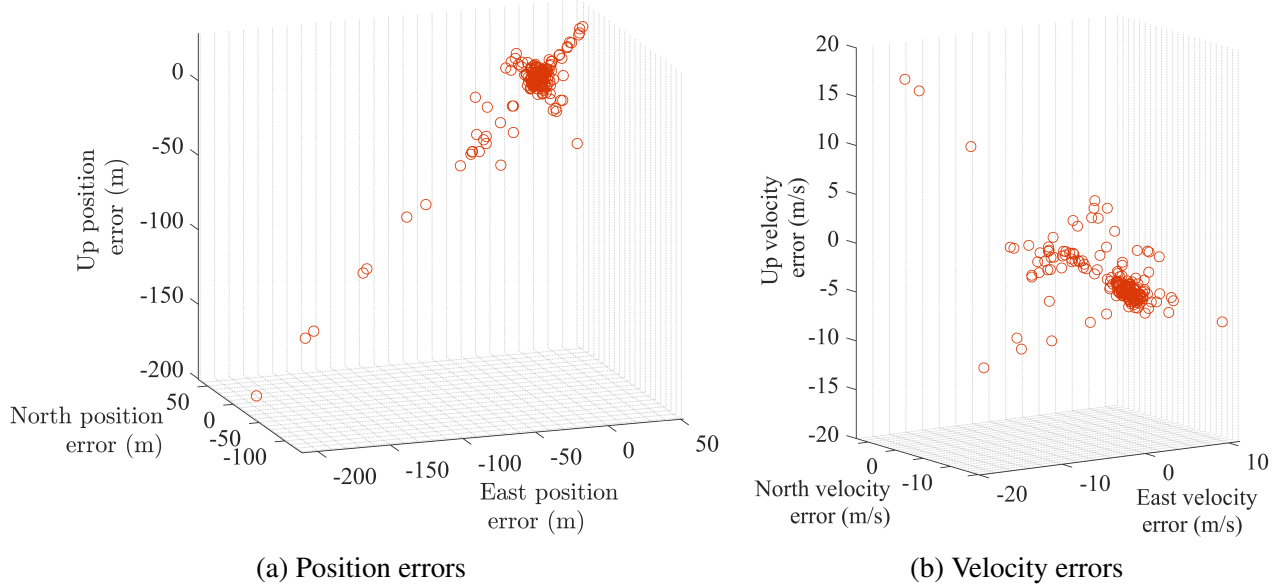


Figure 6: Monte Carlo campaign - Errors with respect to target

of attack is used in the Monte Carlo campaign; we stress that such Guidance is already potentially compatible with online computation requirements. Over a batch of 200 MC runs, the trajectory gets successfully tracked in 199 cases, demonstrating the effectiveness of the proposed lookup table-based method for scheduling the initial conditions of the re-entry burn. However, the poor modelling of gravity force and of apparent forces determines a longer time of flight with respect to the one foreseen within the guidance block. Therefore, as demonstrated in Fig. 6a and in Fig. 6b, the final error with respect to target builds during the last seconds of flight. Nonetheless, the error associated with MECO conditions uncertainty gets handled well, demonstrating the effectiveness of the LUT strategy.

5.2 Online algorithm performance

The algorithm described in Sec. 4 is applied to the re-entry problem for nominal MECO conditions. Notice that the pitch attitude profile presented in this section differs numerically from the ones in Tab. 2, as the guidance algorithm runs on the landing site-centered ENU reference system; however, the attitudes associated with the NED and ENU parameterizations coincide. Number of successive convexifications iterations has been limited to 10: inclusion of the angle of attack constraint, indeed, prevents the algorithm from reaching convergence within its stopping criteria; however, convergence to a physical solution is achieved, therefore this aspect is deemed of minor importance. Excluding the angle of attack constraint, on the other hand, algorithm converges in 3 iterations. Final time is guessed through the convex 3-DoF algorithm; state profiles are guessed as interpolating the prescribed boundary conditions, whereas control profiles are guessed as null. In addition, the control and control rates limitations in Eq. (16), Eq. (17) are included in the optimization process.

$$\mathbf{r}_{\psi,\max} = 5^\circ/s \quad \mathbf{r}_{\theta,\max} = 5^\circ/s \quad \mathbf{r}_{T,\max} = 0.33 (T_{\max} - T_{\min}) N/s \quad (16)$$

$$\dot{\mathbf{r}}_{\psi,\max} = 1^\circ/s^2 \quad \dot{\mathbf{r}}_{\theta,\max} = 1^\circ/s^2 \quad (17)$$

Results of the convergence process for the yaw and pitch profiles and for the thrust magnitude are reported respectively in Fig. 7 and in Fig. 8. It is possible to appreciate how the thrust profile switches

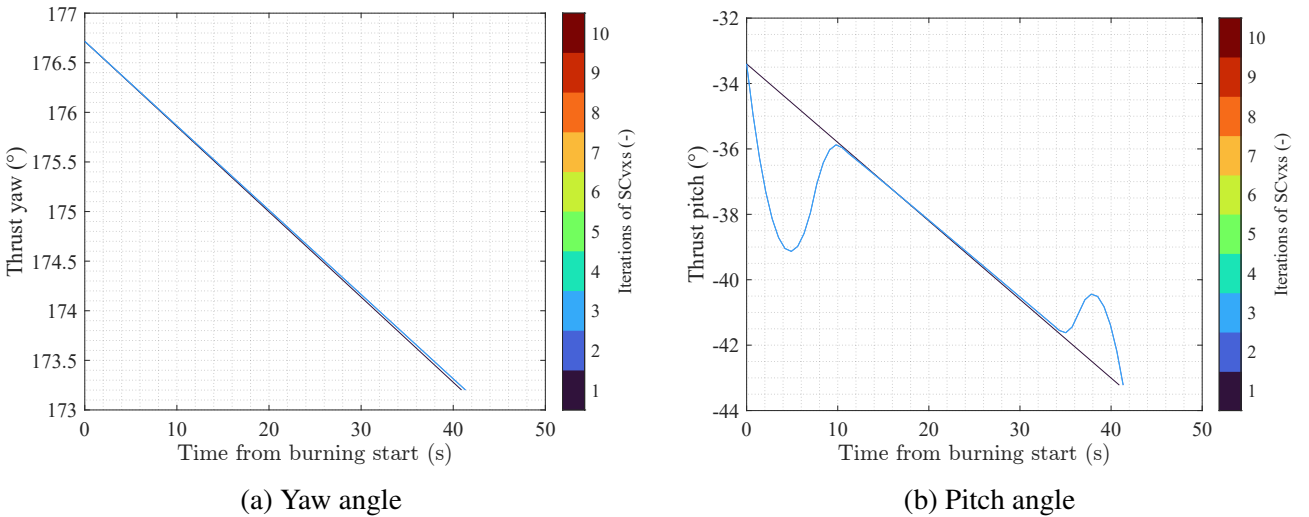


Figure 7: Convergence of thrust angles profiles - *Guidance only*

in only one iteration from a linear trend to a structure resembling a discontinuous *min-max* profile. While yaw profile keeps its linear trend, pitch profile varies in proximity of switches; furthermore, time trend of the pitch profile is upper bounded by the limit on \dot{r}_θ in Eq. (17), as demonstrated by the approximately piecewise-linear behaviour of r_θ , shown in Fig. 9. For what concerns thrust profile, instead, limit on r_T outlined in Eq. (16) is active during thrust magnitude build-up and throttling-down; this makes the resulting thrust profile as close as possible to the theoretical *min-max* structure [34] compatibly with the added control limitations.

At last, the solution is tested in the same high-fidelity simulator employed for the Monte Carlo analysis outlined in the previous subsection. Fig. 11a and Fig. 11b show the evolution through thrusting time respectively of the position and velocity errors in their phase spaces; the fact the errors remain bounded and converge approximately to zero for both velocity and position components demonstrates pragmatically the accuracy of the linearized dynamics treated by the convex solver, besides the convergence of the virtual controls adopted. On the other hand, small residuals on the final errors can

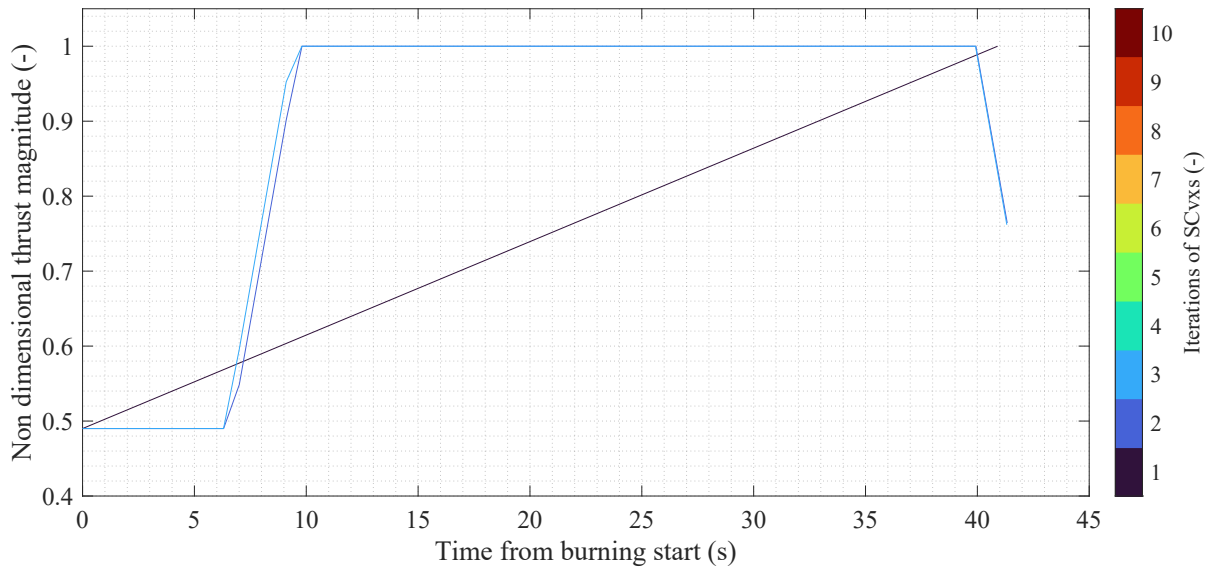


Figure 8: Convergence of non dimensional thrust magnitude profile - *Guidance only*

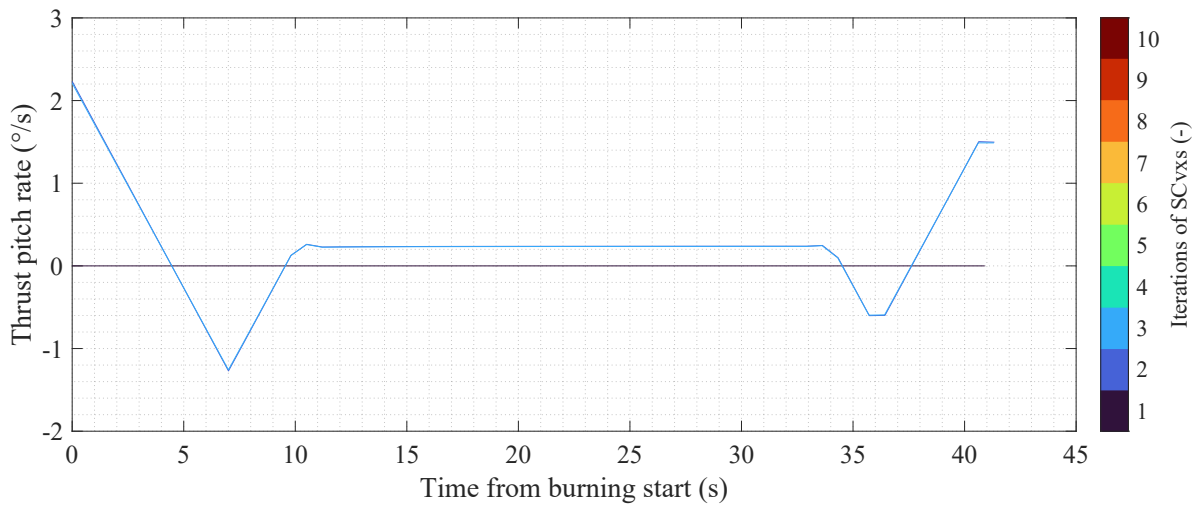


Figure 9: Convergence of thrust pitch rate profile - *Guidance only*

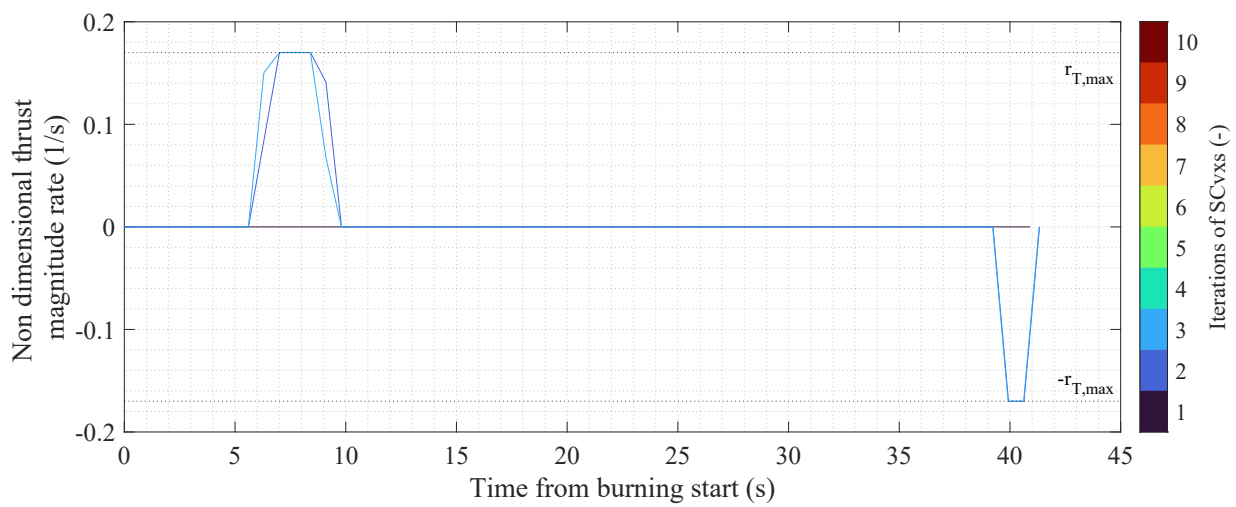


Figure 10: Convergence of non dimensional thrust magnitude rate profile - *Guidance only*

be associated with the discrepancy between final time foreseen by the guidance algorithm and real one, as outlined in Sec. 5.1 as well. It can be indeed noticed that the final time reported on the top of the colorbars of Fig. 11 differs from the one of the profiles computed in the Guidance block, which amounts to approximately 41 s, e.g. visible on the x -axis in Fig. 8. The non-null initial errors are associated with the fact the guidance solution has been implemented in the simulator in open-loop fashion; solution of this aspect, stepping to a closed-loop guidance approach, will further allow testing of the robustness of the proposed AQ5DoF algorithm, as done for the 3DoF one in Sec. 5.1.

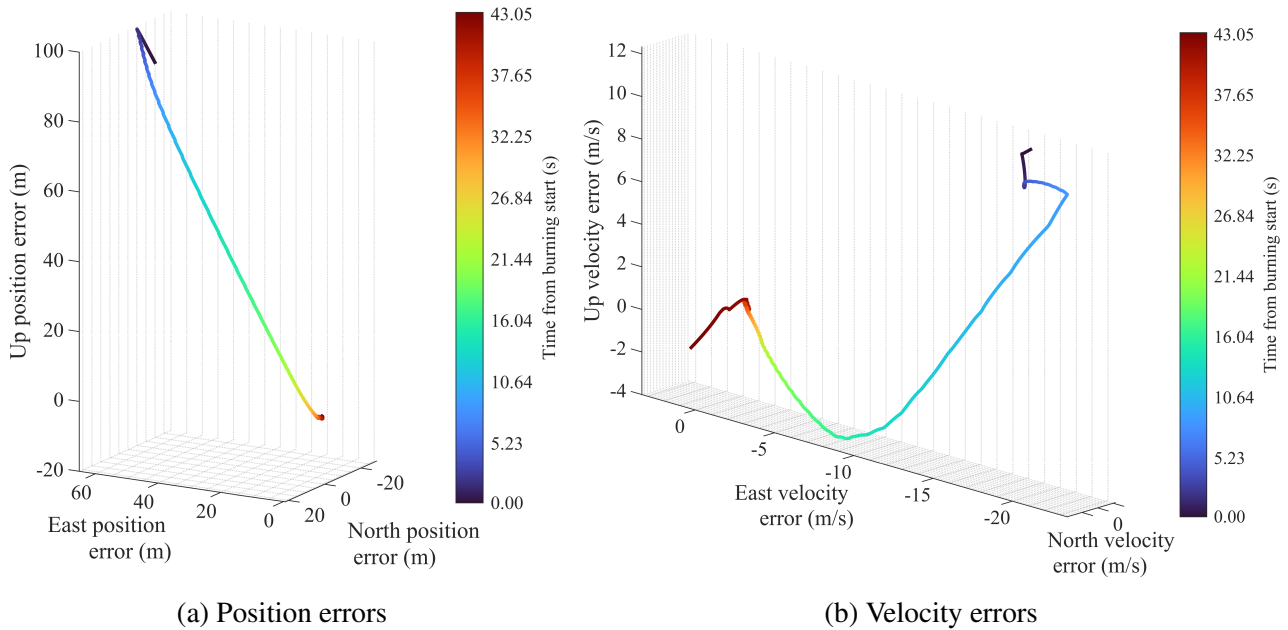


Figure 11: Evolution of errors with respect to reference trajectory using the Augmented Quasi 5DoF guidance scheme - *High-fidelity simulation*

6 CONCLUSIONS AND FUTURE DEVELOPMENTS

A solution for the HAG problem has been proposed in this work, both concerning the re-entry burn scheduling and the online computation of a reference trajectory for the re-entry burn of the high-lift vehicle RETALT1. The scheduling via Lookup Table has demonstrated its effectiveness even accounting for a simplified 3-DoF Guidance in the loop; a hybrid method based on a convex-indirect scheme has been proposed to compile such Lookup Table, providing accurate and fast results; an angle-of-attack limitation has been further included in the LUT to minimize aerodynamic disturbances, through a convex solver. An online scheme for including controller limitations, such as Euler angles and throttling rates, has been proposed and tested for the nominal solution. The scheme has demonstrated correct handling of the SCvxS-associated approximations, as the generated trajectory has been proven to be trackable in a high-fidelity simulation environment.

The first successive step shall include the non linearities associated with gravity in the Guidance scheme, thus providing better estimations of the time of flight. On the other hand, inclusion of the angle of attack constraint in the indirect shooting would make the optimality conditions associated with the ignition height scheduling even more accurate; inclusion of the angle of attack is therefore a desirable development step. At last, the proposed Augmented Quasi 5DoF guidance scheme shall be tested with a Monte Carlo campaign to prove its robustness.

REFERENCES

- [1] Marwege, A. and Gülhan, A. and Klevanski, J. and Hantz, C. and Karl, S. and Laureti, M. and De Zaiacomo, G. and Vos, J. and Jevons, M. and Thies, C. and Krammer, A. and Lichtenberger, M. and Carvalho, J. and Paixão, S., “RETALT: Review of technologies and overview of design changes,” *CEAS Space Journal*, vol. 14, no. 3, Jul. 2022. DOI: 10.1007/s12567-022-00458-9.
- [2] Ghignoni, P. and Botelho, A. and Recupero, C. and Fernandez, V. and Fabrizi, A. and De Zaiacomo, G., “RETALT: Recovery GNC for the Retro-Propulsive Vertical Landing of an Orbital Launch Vehicle,” in *HiSST: 2nd International Conference on High-Speed Vehicle Science Technology (HiSST)*, Zenodo, 2022. DOI: 10.5281/zenodo.7064613.
- [3] Simplício, P. and Marcos, A. and Bennani, S., “Guidance of Reusable Launchers: Improving Descent and Landing Performance,” *Journal of Guidance, Control, and Dynamics*, vol. 42, no. 10, Aug. 2019. DOI: 10.2514/1.G004155.
- [4] Botelho, A. and Martinez, M. and Recupero, C. and De Zaiacomo, G., “Design of the landing guidance for the retro-propulsive vertical landing of a reusable rocket stage,” *CEAS Space Journal*, Feb. 2022. DOI: 10.1007/s12567-022-00423-6.
- [5] Sánchez-Sánchez, C. and Izzo, D., “Real-time optimal control via deep neural networks: Study on landing problems,” *Journal of Guidance, Control, and Dynamics*, vol. 41, no. 5, pp. 1122–1135, 2018. DOI: 10.2514/1.G002357.
- [6] B. Gaudet, R. Linares, and R. Furfaro, “Deep reinforcement learning for six degree-of-freedom planetary landing,” *Advances in Space Research*, vol. 65, no. 7, pp. 1723–1741, 2020, ISSN: 0273-1177. DOI: 10.1016/j.asr.2019.12.030.
- [7] Shen, H. and Seywald, H. and Powell, R. W., “Desensitizing the Minimum-Fuel Powered Descent For Mars Pinpoint Landing,” *Journal of Guidance, Control, and Dynamics*, vol. 33, no. 1, pp. 108–115, 2010. DOI: 10.2514/1.44649.
- [8] Seywald, K. and Seywald, H., “Desensitized optimal control,” in *AIAA Scitech 2019 Forum*. DOI: 10.2514/6.2019-0651.
- [9] Sagliano, M. and Heidecker, A. and Hernández, J. M. and Farì, S. and Schlotterer, M. and Woicke, S. and Seelbinder, D. and Dumont, E., “Onboard Guidance for Reusable Rockets: Aerodynamic Descent and Powered Landing,” in *AIAA Scitech Forum*, Jan. 2021. DOI: 10.2514/6.2021-0862.
- [10] Szmuk, M. and Reynolds, T. P. and Açıkmeşe, B., “Successive convexification for real-time six-degree-of-freedom powered descent guidance with state-triggered constraints,” *Journal of Guidance, Control, and Dynamics*, vol. 43, 2020. DOI: 10.2514/1.G004549.
- [11] Reynolds, T. P. and Szmuk, M. and Malyuta, D. and Mesbahi, M. and Açıkmeşe, B. and Carson, J. M., “Dual quaternion-based powered descent guidance with state-triggered constraints,” *Journal of Guidance, Control, and Dynamics*, vol. 43, no. 9, pp. 1584–1599, 2020. DOI: 10.2514/1.G004536.
- [12] Kamath, A. G. and Elango, P. and Kim, T. and Mceowen, S. and Yu, Y. and Carson, J. M. and Mesbahi, M. and Açıkmeşe, B., “Customized real-time first-order methods for onboard dual quaternion-based 6-dof powered-descent guidance,” in *AIAA SCITECH 2023 Forum*. DOI: 10.2514/6.2023-2003.
- [13] Berning, A. W. and Strohl, L. and Bieniawski, S. R., “Lossless convex guidance for lunar powered descent,” in *AIAA SCITECH 2023 Forum*. DOI: 10.2514/6.2023-2004.

- [14] Ridderhof, J. and Tsiotras, P. and Johnson, B. J., “Stochastic entry guidance,” *Journal of Guidance, Control, and Dynamics*, vol. 45, no. 2, pp. 320–334, 2022. DOI: 10.2514/1.G005964.
- [15] Bonalli, R. and Lew, T. and Pavone, M., “Sequential convex programming for non-linear stochastic optimal control,” *ESAIM: COCV*, vol. 28, p. 64, 2022. DOI: 10.1051/cocv/2022060.
- [16] Mao, Y. and Szmuk, M. and Aıkmee, B., “Successive convexification of non-convex optimal control problems and its convergence properties,” in *2016 Conference on Decision and Control*, IEEE, Dec. 2016. DOI: 10.1109/cdc.2016.7798816.
- [17] Malyuta, D. and Reynolds, T. and Szmuk, M. and Mesbahi, M. and Aıkmee, B. and Carson, J., “Discretization performance and accuracy analysis for the rocket powered descent guidance problem,” in *AIAA Scitech Forum*, Jan. 2019. DOI: 10.2514/6.2019-0925.
- [18] Blackmore, L. and Aıkmee, B. and Scharf, D. P., “Minimum-Landing-Error Powered-Descent Guidance for Mars Landing Using Convex Optimization,” *Journal of Guidance, Control, and Dynamics*, vol. 33, no. 4, Aug. 2010. DOI: 10.2514/1.47202.
- [19] Kamath, A. G. and Elango, P. and Yu, Y. and Mceowen, S. and Carson III, J. M. and Aıkmee, B., *Real-Time Sequential Conic Optimization for Multi-Phase Rocket Landing Guidance*, 2022. arXiv: 2212.00375.
- [20] Spada, F. and Sagliano, M. and Topputo, F., “Direct-Indirect Hybrid Strategy for Optimal Powered Descent and Landing,” *Journal of Spacecraft and Rockets*, Accepted for publication. DOI: 10.2514/1.A35650.
- [21] Zhang, C. and Topputo, F. and Zhao, Y., “Low-Thrust Minimum-Fuel Optimization in the Circular Restricted Three-Body Problem,” *Journal of Guidance, Control, and Dynamics*, vol. 38, no. 8, Aug. 2015. DOI: 10.2514/1.G001080.
- [22] Sagliano, M., “Generalized *hp* Pseudospectral-Convex Programming for Powered Descent and Landing,” *Journal of Guidance, Control, and Dynamics*, vol. 42, no. 7, Jul. 2019. DOI: 10.2514/1.G003731.
- [23] D. Garg, M. Patterson, C. Francolin, *et al.*, “Direct Trajectory Optimization and Costate Estimation of Finite-Horizon and Infinite-Horizon Optimal Control Problems via a Radau Pseudospectral Method,” *Computational Optimization and Applications*, vol. 49, Jan. 2011. DOI: 10.1007/s10589-009-9291-0.
- [24] Aıkmee, B. and Casoliva, J. and Carson, J. M. and Blackmore, L., “G-FOLD: A Real-Time Implementable Fuel Optimal Large Divert Guidance Algorithm for Planetary Pinpoint Landing,” in *Concepts and Approaches for Mars Exploration*, LPI Editorial Board, Ed., ser. LPI Contributions, 2012.
- [25] Blackmore, L., “Autonomous precision landing of space rockets,” in *Frontiers of Engineering: Reports on Leading-Edge Engineering from the 2016 Symposium*, vol. 46, Washington, DC: The National Academies Press, 2017. DOI: 10.17226/23659.
- [26] Aıkmee, B. and Ploen, S. R., “Convex Programming Approach to Powered Descent Guidance for Mars Landing,” *Journal of Guidance, Control, and Dynamics*, vol. 30, no. 5, 2007. DOI: 10.2514/1.27553.
- [27] Fahroo, F. and Ross, I. M., “Costate Estimation by a Legendre Pseudospectral Method,” *Journal of Guidance, Control, and Dynamics*, vol. 24, no. 3, Apr. 2001. DOI: 10.2514/2.4709.

- [28] Domahidi, A. and Chu, E. and Boyd, S., “ECOS: An SOCP Solver for Embedded Systems,” in *European control Conference (ECC)*, 2013. DOI: 10.23919/ECC.2013.6669541.
- [29] Taheri, E. and Arya, V. and Junkins, J. L., “Costate mapping for indirect trajectory optimization,” *Astrodynamics*, vol. 5, Dec. 2021. DOI: 10.1007/s42064-021-0114-0.
- [30] Bryson, A. E. and Ho, Y., *Applied Optimal Control - Optimization, Estimation and Control*. Taylor & Francis, 1975.
- [31] Pontryagin, L.S., *The Mathematical Theory of Optimal Processes*. John Wiley & Sons, 1962.
- [32] Betts, J. T., “Survey of Numerical Methods for Trajectory Optimization,” *Journal of Guidance, Control, and Dynamics*, vol. 21, no. 2, Apr. 1998. DOI: 10.2514/2.4231.
- [33] Russell, R. P., “Primer Vector Theory Applied to Global Low-Thrust Trade Studies,” *Journal of Guidance, Control, and Dynamics*, vol. 30, no. 2, 2007. DOI: 10.2514/1.22984.
- [34] Lu, P., “Propellant-optimal powered descent guidance,” *Journal of Guidance, Control, and Dynamics*, vol. 41, pp. 1–14, Dec. 2017. DOI: 10.2514/1.G003243.